RSC Advances

PAPER

View Article Online
View Journal | View Issue

Cite this: *RSC Adv.*, 2014, **4**, 19925

$BiFeO_3$/YSZ bilayer electrolyte for low temperature solid oxide fuel cell†

Yu-Chieh Tu,[a] Chun-Yu Chang,[a] Ming-Chung Wu,[b] Jing-Jong Shyue[ac] and Wei-Fang Su*[a]

Received 3rd March 2014
Accepted 17th April 2014

DOI: 10.1039/c4ra01862a

www.rsc.org/advances

We have demonstrated $BiFeO_3$ (BFO) as a potential bilayer electrolyte for 650 °C low temperature solid oxide fuel cell application. The stoichiometric perovskite BFO is synthesized by wet chemistry, calcined at 500 °C and sintered at 850 °C. The crystalline structure is confirmed by X-ray diffraction spectroscopy, the atomic ratios (Bi : Fe) of 1.02 and 1.00 are determined by X-ray energy dispersive spectroscopy and inductively coupled plasma-mass spectroscopy, respectively. The X-ray photoelectron spectroscopy analysis indicates the presence of oxygen vacancies which can partially reduce Fe^{3+} and result in relatively high dielectric constant (6252 at 100 kHz) and ionic conductivity (>10^{-2} S cm^{-1} at 650 °C). The BFO is coated with an yttria-stabilized zirconia (YSZ) protective layer to avoid hydrogen reduction of BFO. This bilayer electrolyte exhibits a 1.6 times increase in maximum power density as compared with pure YSZ when a Ni–YSZ anode and lanthanum strontium cobalt ferrite (LSCF) cathode are used in the fuel cell at 650 °C.

Introduction

The solid oxide fuel cell (SOFC) is one of the promising clean energy sources in the 21st century.[1–5] At present, an yttria stabilized zirconia (8 mol% Y_2O_3 in ZrO_2, YSZ) electrolyte has been widely used in the SOFC due to its high ionic conductivity, and good chemical and mechanical stability.[6,7] However, the SOFC using YSZ electrolyte has to be operated at a high temperature of >700 °C.[8] The high operation temperature consumes energy to maintain it and requires expensive high temperature resistant interconnects.[9,10] Thus, there is urgent need to develop new electrolyte material that has high ionic conductivity at low temperature of 650 °C or below. Recently, bismuth based materials have been identified as good low temperature electrolytes due to the ease of ionization of bismuth.[11–13] The fluorite-type bismuth oxides such as Er doped Bi_2O_3(ESB),[14] Dy_2O_3/WO_3-doped Bi_2O_3(DWSB),[15] $Bi_4YbO_{7.5}$ (ref. 16) were reported as low temperature solid oxide electrolytes for fuel cell. However, they contain very expensive rare element. The low cost perovskite $BiFeO_3$ (BFO) would be a good candidate for low cost and low temperature oxide electrolyte because ionic radius of Bi and Fe are large to accommodate oxygen vacancies for high ionic conductivity. The BFO is a rhombohedrally distorted perovskite structure with ferroelectricity and antiferromagnetism, and widely used in gas sensors, data storage, microelectronic devices, and visible-light photocatalyst.[17–22] The perovskite BFO can be prepared using various methods such as solid state reaction process,[23–27] pulsed layer deposition,[28] epitaxial growth[17] and sol–gel synthesis.[29] It is difficult to synthesize pure phase BFO using solid state reaction process due to the formation of second phase. The second phase can be etched away by nitric acid[24] or reduced by a rapid liquid phase sintering process at 880 °C.[25] In this study, we report a stoichiometry controlled BFO powder was synthesized by low cost solution method and then sintered at 850 °C to obtain pure perovskite structure. We demonstrate the BFO powder can be fabricated into a bilayer electrolyte (YSZ coated BFO) for the use of 650 °C fuel cell.

Experimental details

The chemicals and materials were used as received without further purification including bismuth nitrate pentahydrate (Lot: MKBG7332V, 98%, Aldrich), iron nitrate nonahydrate (Lot: STBC2273V, 98%, Aldrich), 2-ethoxyethanol (Lot: A0298235, 99%, Acros), acetic acid (Lot: J15805, J. T. Baker), polyvinyl alcohol binder (PVA, Lot: MKBD2298, 80%, Aldrich), ZrO_2-8% mole Y_2O_3 powder (YSZ, Tosoh Corporation), nickel oxide powder (NiO, Alfa Aesar), graphite powder (Lot: H24X012, 99.9999%, Alfa Aesar), α-terpineol (Alfa Aesar), ethyl cellulose (Acros), lanthanum strontium cobalt ferrite (LSCF) slurry

[a]*Department of Materials Science and Engineering, National Taiwan University, No. 1, Sec. 4, Roosevelt Road, Taipei 10617, Taiwan. E-mail: suwf@ntu.edu.tw; Fax: +886 2 33664078; Tel: +886 2 33664078*

[b]*Department of Chemical and Materials Engineering, Chang Gung University, No. 259, Wen-Hwa 1st Road, Taoyuan 333-02, Taiwan*

[c]*Research Center for Applied Sciences, Academia Sinica, No. 128, Sec. 2, Academia Road, Taipei 11529, Taiwan*

† Electronic supplementary information (ESI) available. See DOI: 10.1039/c4ra01862a

($La_{0.6}Sr_{0.4}Co_{0.2}Fe_{0.8}O_{3-\delta}$, Fuel Cell Materials Corporation), and silver paste (TED PELLA).

The BFO was synthesized using excess Bi at a composition of Bi/Fe = 1.05/1.00 to compensate the volatility of bismuth during the sintering process. In a 500 ml three neck flask, 10.1865 g (0.021 mol) of bismuth nitrate pentahydrate and 8.0805 g (0.020 mol) of iron nitrate nonahydrate were dissolved in a mixture of 200 ml of 2-ethoxyethanol and 200 ml of acetic acid at 70 °C for 30 min in Ar to obtain a clear yellow brown BFO precursor solution. The BFO precursor solution was dried at 120 °C overnight to obtain BFO powder. The BFO was calcined in air by heating it to 500 °C at 10 °C min^{-1} and then kept at 500 °C for 2 h to obtain calcined powder. After grinding and sieving, the calcined BFO powder has an average particle size of 177 nm which was determined by dynamic light scattering method (3000 HAS Zetasizer, Malvern Instrument). A combined instrument (SDT-Q600, TA Instrument) of thermogravimetric analyzer (TGA) and differential scanning calorimetry (DSC) was used to determine the decomposition temperature of organic component and the phase transition temperature of BFO respectively. The 6.6 mg of as-synthesized BFO was heated from room temperature to 825 °C at 10 °C min^{-1} in air to obtain the thermal behaviors of BFO.

Disks with and without PVA were fabricated for the characterization of sintered BFO. For the disk containing PVA, the 500 mg of calcined powder was mixed with 1.0 wt% PVA binder, and pressed into a disk of 10 mm in diameter under a uniaxial force of 20 kg cm^{-3} for 20 s, and then 50 kg cm^{-3} for 2 min. The BFO disk was sintered from room temperature (RT) to 550 °C at 2 °C min^{-1} and then kept at 550 °C for 4 h in air to remove PVA. And then the disk was heated further from 550 °C to higher temperature *e.g.*, 750 °C, 800 °C, 850 °C, and 900 °C at 1 °C min^{-1}, respectively and kept at that temperature for 4 h. At the end of holding time, the power of furnace was switched off and the sintered disk was naturally cooled inside the furnace. The sintered BFO disk was used for the measurement of density and dielectric constant. For the disk without PVA, the same sintering processes was used, the sample was used for determining its crystalline structure, morphology, ionic conductivity and power density.

The experimental density of different BFO disks was measured by using Archimedes' method. The relative density of BFO disk was calculated basis on the theoretical density of 8.346 g cm^{-3} by assuming a rhombohedral distorted perovskite structure.[30] The crystal structure of BFO disks was determined by X-ray diffraction spectrometry (XRD) (Rigaku, TTRAXIII) using Cu K_α radiation at 50 kV and 300 mA. XRD patterns were collected from 2θ between 20 and 70 with a 0.005° step at 5° min^{-1}. The morphology of BFO disks were studied by scanning electron microscopy (SEM) (JEOL, JSM-6510). Inductively coupled plasma-mass spectroscopy (ICP-MS) (7500ce, Agilent, Japan) and X-ray energy dispersive spectroscopy (EDS) attached to SEM were used to determine the ratio of Bi to Fe in the sintered BFO. The X-ray photoelectron spectrometry (XPS) (ULVAC-PHI, Chigasaki, Japan) was used to examine the core-levels of BFO disk by using Al K_α radiation with a photoelectron take off angle of 45° in high vacuum ($\sim 10^{-7}$ torr). The relative dielectric constant and dielectric loss were measured by using inductance–capacitance–resistance (LCR) (Wayne Kerr 6420) meter at 10 kHz and 100 kHz frequencies respectively.

A direct current four-probe configuration was used for the measurement of ionic conductivity using Teraoka's method.[31,32] The multilayer sample of Ag/LSCF/YSZ/BFO/YSZ/LSCF/Ag was used for the measurement. The preparation of each layer is described in the following. The BFO layer was prepared by pressing BFO calcined powder in a rectangular mold with a dimension of 0.4 × 0.4 × 4.5 cm^3 first and then sintered at 850 °C for 4 hours. The two YSZ layers were made from plates with the dimension of 0.4 × 0.4 × 0.1 cm^3 which were prepared respectively by pressing YSZ powder under a uniaxial force of 10 kg cm^{-3} for 10 s in a mold, then sintered the samples from room temperature to 1400 °C at a rate of 2 °C min^{-1} and held at this temperature for 4 h. The 40–50 micron of LSCF was screened printed on each YSZ plate to make LSCF coated YSZ plates and sintered from room temperature to 850 °C at 5 °C min^{-1} and then kept at 850 °C for 4 h in air. Then all the layer parts were clamped together into a sample holder and connected to the Keithley 2410 electrometer by silver wires for ionic conductivity measurement at a constant current of 10 mA in the temperature range of 823–973 K.

The electromotive force (EMF) was used to determine the ionic transport number (t_i) accordingly to the literature.[33] The sample was fabricated by depositing 150 nm thin platinum electrode on both side of 1.1 mm thick BFO disk and then sintered at 850 °C and connected to the voltage/ampere meter using silver wire for measurements. The t_i was measured from 200 °C to 650 °C using gradient oxygen concentration, one side is air ($pO_2 = 0.21$ atm) and the other side is pure oxygen ($pO_2 =$ 1.00 atm). The t_i can be obtained from the ratio of the measured emf (E_{exp}) and theoretical Nernst voltage (E_{th}) as shown in eqn (1).

$$t_i = \frac{E_{exp}}{E_{th}} \quad (1)$$

The fuel cell has a multilayer structure of anode/protective layer YSZ/BFO/cathode which is fabricated by step-wise procedure to ensure high mechanical strength without cross contamination. The procedure was described in the following. For the anode of fuel cell, 0.8 g of YSZ powder, 1.2 g of nickel oxide powder and 0.2 g of graphite powder were first milled for 1 h to prepare Ni–YSZ powder. The 300 mg of Ni–YSZ powder were pressed into a disk of 14 mm diameter under a uniaxial force of 40 kg cm^{-3} for 60 s, and then an YSZ protective layer was coated on the top of disk by spinning YSZ slurry at 6000 rpm for 60 s. To form the stable YSZ slurry, 7.8 g of YSZ powder, 0.5 g of ethyl cellulose and 17.0 g of α-terpineol were mixed and ball milled for two days. The assembled anode was sintered from RT to 1400 °C at 2 °C min^{-1} and then kept at 1400 °C for 4 h in air. For the electrolyte layer of BFO, the 500 °C calcined BFO powder was mixed first with 93.0 g of α-terpineol and 7.0 g of ethyl cellulose. The resulting BFO slurry was coated onto the anode by casting. The BFO coated anode was dried at RT and then sintered to 850 °C at 2 °C min^{-1} and then kept at 850 °C for 4 h in air. Then,

the LSCF cathode layer was coated by screen printing on top of BFO layer using lanthanum strontium cobalt ferrite (LSCF) slurry to finish the assembly of fuel cell. The assembled fuel cell was sintered from RT to 850 °C at 5 °C $min^{-1}$and then kept at 850 °C for 2 h in air. The final sintered fuel cell has the structure of Ni–YSZ/YSZ/BFO/LSCF at the thickness of 550 μm/17 μm/30 μm/44 μm, respectively. The thickness of YSZ electrolyte in the pure YSZ cell is 18 μm.

Results and discussion

We prepared perovskite BFO using a simple solution method. The BFO powder was synthesized first by reacting bismuth nitrate and iron nitrate in a mixture of 2-ethoxyethanol and acetic acid at 70 °C for 30 min and dried at 120 °C overnight. To control the stoichiometry of the BFO, the raw material molar ratio of Bi/Fe at 1.05/1.00 was used to compensate the volatility of bismuth during the sintering process. As shown in Fig. 1, the BFO powder started to lose weight at 162 °C (black TGA curve) and indicated the first rapid weight loss at 206 °C (blue DSC curve) which were due to the elimination of water from polyvinyl alcohol binder. The second rapid weight loss at 276 °C (DSC curve) was due to the rupture of carbon–hydrogen bond and carbon–carbon bond. The third peak of the DSC curve at 400 °C was the residual carbon changed to carbon dioxide.[34] The forth exothermic peak at 800 °C (DSC curve) was due to the crystallization of BFO.

According to the results of thermal analysis, we calcined BFO powder at 500 °C for two hours before any further thermal treatment. To study the crystallization behaviour and optimal sintering temperature of BFO, the calcined powder was thermally treated at different temperature and the results are shown in Fig. 2. The perovskite BFO already formed in the calcined powder with iron rich impurity of $Bi_2Fe_4O_9$ (JCPDS no. 721832). The purity of BFO was improved further upon heat treatment at higher temperature. After 800 °C treatment, the good quality of crystal was formed with minute bismuth rich impurity of $Bi_{36}Fe_2O_{57}$ (JCPDS no. 420181). A pure perovskite BFO was obtained for sample sintered at either 850 °C or 900 °C.

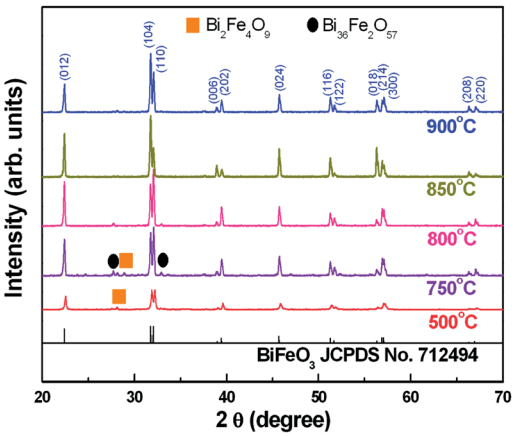

Fig. 2 XRD patterns of BFO samples prepared at different temperature.

The changes of BFO densification were monitored by measuring the density of each sample sintered at different temperature and shown in Fig. 3. A close to 92% of theoretical density was achieved for the 850 °C sample. The morphology changes of samples at different temperature were studied by SEM as shown in Fig. 4. The results indicated the grain sizes of samples were increased and the porosity was decreased after increasing the sintering temperature.

The chemical composition of BFO was initially studied by EDS for samples sintered at different temperature. For the 750 °C sample, the ratio of Bi/Fe is the same as the reactants at 1.05. However, the ratio was decreased to close to 1.00 for the 900 °C sample. The elemental analysis of EDS is usually biased toward the heavier element. The analysis of Bi/Fe ratio was further studied by more accurate ICP-MS analysis. The results indicate the stoichiometry ratio of 1.00 was achieved after thermal treatment at 850 °C. The physical and chemical characteristics of BFO samples prepared at different temperature are summarized in Table 1.

The oxygen binding energies of the BFO after different temperature treatment were investigated by XPS and the results

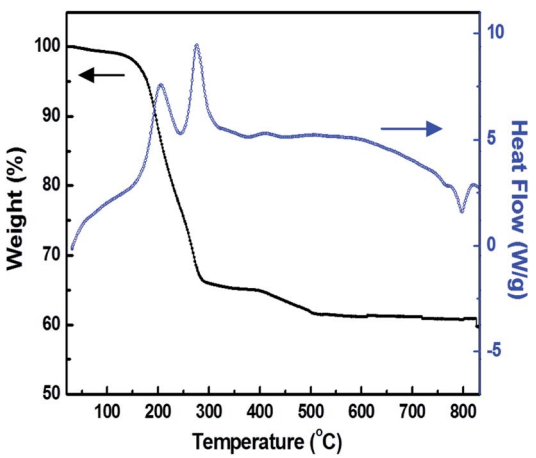

Fig. 1 TGA and DSC curves of BFO powder.

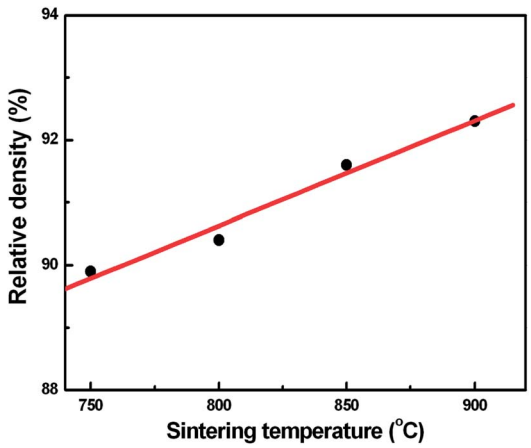

Fig. 3 Relative density (fitted spectra: red solid line) of BFO samples prepared at different temperature.

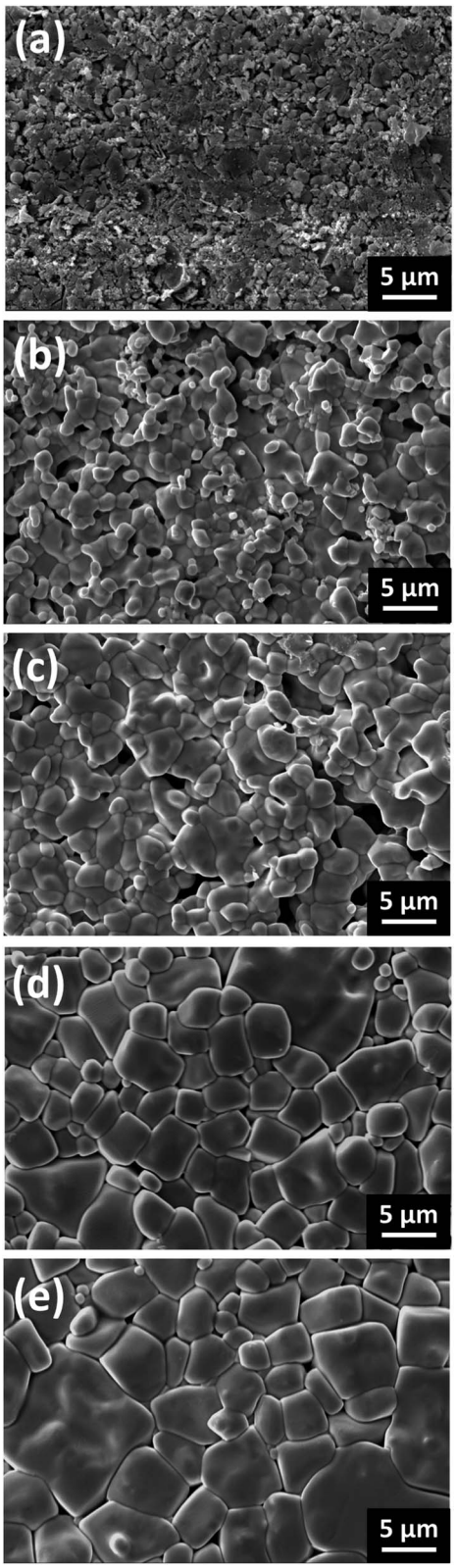

Fig. 4 SEM images of BFO samples prepared at different temperature: (a) 500 °C, (b) 750 °C, (c) 800 °C, (d) 850 °C, and (e) 900 °C.

are shown in Fig. 5. The O 1s binding[35] of BFO at 529 eV is clearly observed for all samples. It is interested to note that oxygen vacancy (V_o^{2+}) at 532 eV was also present in all samples. The oxygen vacancy may be produced from the removal of OH^-, NO_3^- during the sintering process,[36] it was reduced somewhat with increasing sintering temperature above 500 °C. It is known the amount of oxygen vacancies is directly related to the conductivity of electrolyte.[37] However, the sample sintered at 500 °C did not form pure perovskite BFO with high density. High quality electrolyte should have high density to minimize the potential gas crossover, so the samples sintered at 850 °C and 900 °C were evaluated for the application of electrolyte.

The iron binding energies[38] of BFO prepared at different temperature were further investigated by XPS as shown in Fig. 6. The measured curve was fitted under a linear background black dash-dot line between 62.8 eV and 50 eV. Fig. 6 clearly shows two characteristic peaks appearing at 55.6 eV for Fe^{3+} and 53.8 eV for Fe^{2+}, respectively. These results show the coexistence of Fe^{3+} and Fe^{2+} is easily formed in our samples due to the presence of oxygen vacancy according to the following reaction.

$$4Fe^{3+} + O^{2-} \rightarrow 4Fe^{2+} + V_o^{2+} + 1/2O_2 \quad (2)$$

The distorted structure of BFO results in high dielectric constant in the range of several hundred depending on the preparation method. We measured the dielectric constant and dielectric loss of our solution method prepared BFO samples sintered at different temperature and the results are summarized in Table 2. It was worth noting they all exhibit rather high dielectric constant and dielectric loss as compared with conventional solid state method and thin film deposition method. The results can be deduced from the presence of high oxygen vacancy in our samples as shown in the XPS study. The abnormal high dielectric constant and loss may suggest the material may have high ionic mobility.

The material requirements for high ionic conductivity solid oxide electrolyte material are (1) available empty sites, and (2) low energy barrier for ions to hop.[37] The ionic mobility of material can be expressed by two kinds of values: ionic conductivity[31,32] and ionic transport number.[33] We measured the changes of ionic transport number from 200 °C to 650 °C and ionic conductivity from 550 °C to 700 °C for the BFO samples sintered at 850 °C. The sample sintered below or above this temperature was not used due to the impurity presence in the former and the high energy usage in the later. Fig. 7 shows the ionic transport number approaches 0.99 at 650 °C which indicates the BFO is ionized at this temperature. Fig. 8 shows the ionic conductivity of BFO is 7.9×10^{-2} S cm^{-1} at 650 °C. The

Table 1 Characteristics of BFO samples prepared at different temperature

Temperature (°C)	Density (g cm^{-3})	Grain size (μm)	Atomic ratio of Bi/Fe by EDS, and ICP-MS in parentheses
750	7.510	1.75	1.05
800	7.553	2.46	1.04, (1.01)
850	7.649	4.50	1.02, (1.00)
900	7.708	6.04	1.01

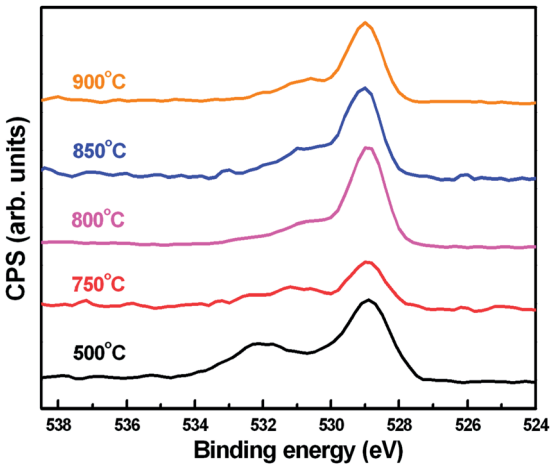

Fig. 5 XPS spectra of O 1s binding energy of BFO samples prepared at different temperature.

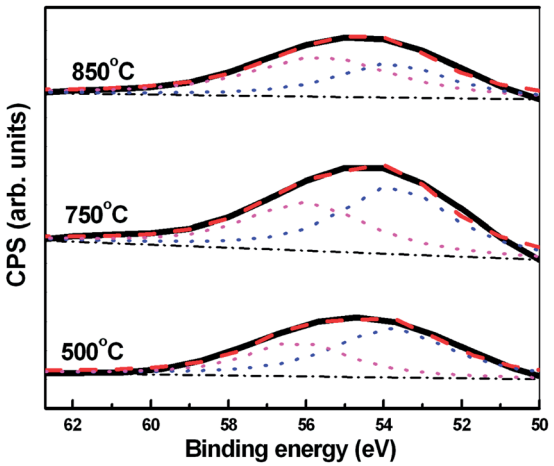

Fig. 6 XPS spectra (measured spectra: black solid lines, fitted spectra: red dash lines) of Fe 3p binding energy of BFO samples prepared at different temperature.

plot of $\ln(\sigma T)$ *vs.* 1000/T is linear which can be expressed by Arrhenius equation[39] as shown in eqn (3).

$$\sigma = \frac{A}{T}\exp\left(-\frac{E_{a,ion}}{kT}\right) \quad (3)$$

where σ is the ionic conductivity, T is the absolute temperature, k is the Boltzmann constant, A is the pre-exponential factor, and $E_{a,ion}$ is the ionic activation energy. Thus, the ionic activation

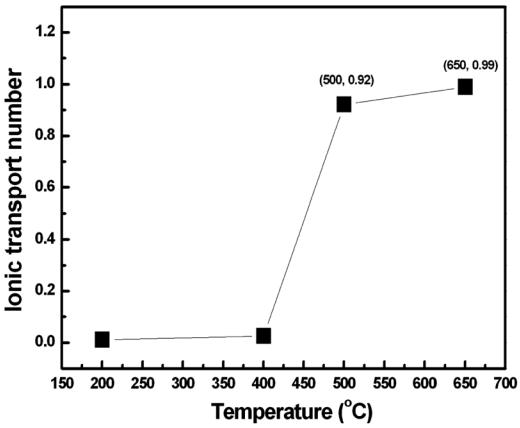

Fig. 7 Plot of oxygen transport number *versus* temperature for BFO sample prepared at 850 °C.

energy of BFO can be determined from the slope of the plot to be 0.69 eV which is lower than the ionic activation energy of YSZ of 1.01 eV.[39] Thus, the BFO should be a good electrolyte material for low temperature SOFC due to its relatively high ionic conductivity at 650 °C and low ionic activation energy.

We found the fuel cell fabricated from the BFO only electrolyte exhibited both low open-circuit voltage and low power density as shown in Fig. S1 of ESI.† The Bi content of BFO was reduced from 18 at% to 2.74 at% without YSZ layer after the fuel cell operated at 700 °C (Table S1†). The large amount of Bi^{3+} in BFO was changed to Bi and separated from BFO upon hydrogen exposure; the grain size of BFO become much smaller as shown in the SEM study (Fig. S2†). Thus, we made a functionally graded bilayer electrolyte by placing a hydrogen inert layer of YSZ on the top of BFO layer to protecting it from contacting with hydrogen. Here, the YSZ serves dual functions: protective layer and electrolyte layer. The fuel cell was assembled from Ni–YSZ anode, YSZ/BFO bilayer electrolyte, and lanthanum strontium cobalt ferrite (LSCF) cathode. Fig. 9(a) and (b) show the cross-sectional SEM photos of the fuel cell using YSZ electrolyte and BFO electrolyte. The thickness of YSZ/BFO bilayer electrolyte is 17 μm/30 μm. The performance of fuel cells with and without BFO was measured at 500 °C, 550 °C, 600 °C, 650 °C and 700 °C respectively. The results are shown in Fig. 10. At 500 °C as expect, the maximum power density of YSZ/BFO electrolyte solar cell has been improved as compared with pure YSZ electrolyte which is consistent with the results of oxygen transport number study. However, both samples exhibits low power density in the range of 14–50 mW

Table 2 Dielectric constant and dielectric loss of BFO samples prepared at different temperature

Temperature (°C)	Dielectric constant at 10 kHz	Dielectric loss at 10 kHz	Dielectric constant at 100 kHz	Dielectric loss at 100 kHz
750	3443	0.11	3027	0.44
800	3459	0.16	2940	0.59
850	7477	0.18	6252	0.52
900	7355	0.19	6104	0.47

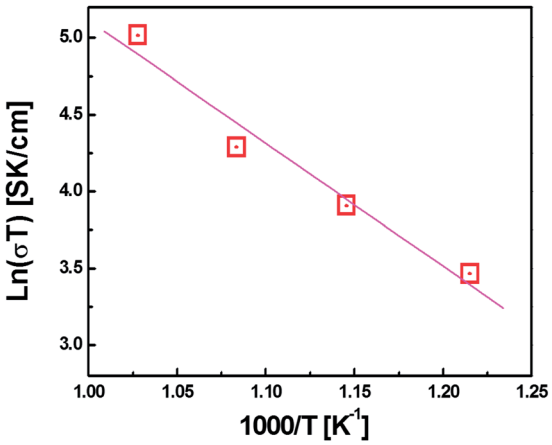

Fig. 8 Plot of ionic conductivity *versus* temperature for BFO sample prepared at 850 °C.

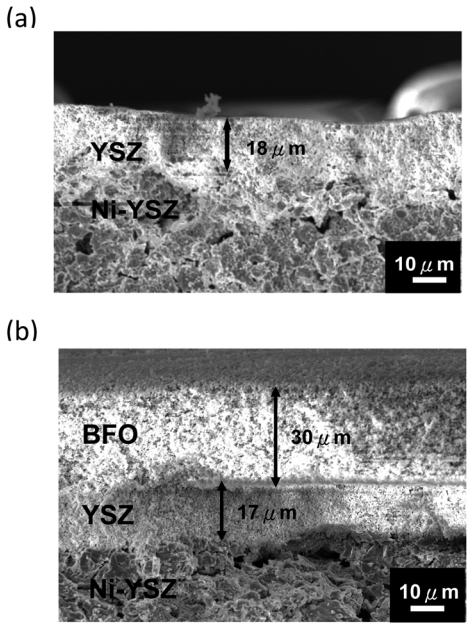

Fig. 9 Cross-sectional SEM photos of fuel cell with (a) YSZ electrolyte and (b) YSZ/BFO electrolyte.

cm^{-2}. The power density of fuel cell with the BFO/YSZ was increased when the operating temperature increasing above 500 °C. At 650 °C, it has shown more than 1.6 times increase in power density as compared with the fuel cell with YSZ only. In the present configuration of fuel cell with BFO/YSZ, the actual electrolyte is BFO and the YSZ serves as a protective layer only. The result is very promising and suggests the solution method prepared BFO electrolyte has potential application for low temperature solid oxide fuel cell. As indicates in Fig. 10, the open-circuit voltage (OCV) of YSZ/BFO electrolyte is lower than pure YSZ electrolyte which may be from the minute reduction of Bi^{3+} of BFO to Bi. When we increased the thickness of YSZ layer from ~17 micron to ~100 micron, the open circuit voltage remained above 1.0 V but the power density was

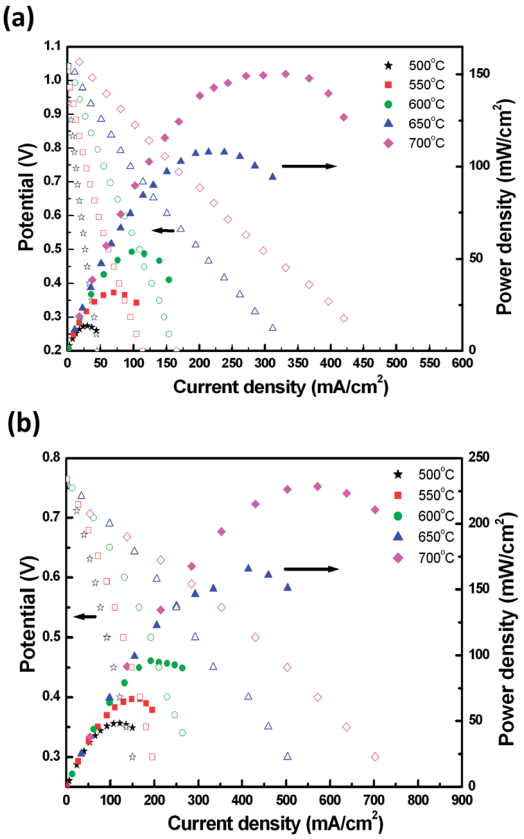

Fig. 10 Comparison of fuel cells performance with (a) YSZ electrolyte and (b) YSZ/BFO electrolyte at different operating temperature.

decreased from 175 mW cm^{-2} to 45 mW cm^{-2} at 650 °C (Fig. S3†). That is due to poor ionic conductivity of YSZ dominating the performance of fuel cell. To reach both high power density and high open-circuit voltage of BFO fuel cell, it is possible using more densed thin YSZ protective layer and higher ionic conductivity of novel doped BFO.

Conclusion

We have successfully demonstrated the low cost solution method to prepare BFO which has potential application as electrolyte for low temperature solid oxide fuel cell. The BFO powder was first prepared using bismuth nitrate and iron nitrate in a mixture of 2-ethoxyethanol and acetic acid at 70 °C. The optimal sintering temperature of BFO was determined to be 850 °C which shows the material is in pure perovskite structure, 92% densification, the Bi/Fe ratio of 1.00, ionic conductivity of 7.9×10^{-2} S cm^{-1} at 650 °C and ionic activation energy of 0.69 eV. The sintered BFO exhibits high oxygen vacancy that results in high dielectric constant and high ionic conductivity. The fuel cell was assembled from Ni–YSZ anode, YSZ/BFO bilayer electrolyte, and lanthanum strontium cobalt ferrite cathode. The maximum power density of fuel cell with YSZ/BFO electrolyte was increased by 1.6 times as compared with pure YSZ electrolyte. The power density could be improved further using high ionic conductivity novel doped BFO.

Acknowledgements

The authors thank the Ministry of Science and Technology of Taiwan (101-2120-M-002-003, 102-3113-P-002-027 and 102-2120-M002-010) for financial support of this research.

Notes and references

1 S. D. Souza, S. J. Visco and L. C. D. Jonghe, *Solid State Ionics*, 1997, **98**, 57.
2 J. P. P. Huijsmans, F. P. F. V. Berkel and G. M. Christie, *J. Power Sources*, 1998, **71**, 107.
3 B. C. H. Steele, *Solid State Ionics*, 2000, **129**, 95.
4 Z. Jiang, L. Zhang, L. Cai and C. Xia, *Electrochim. Acta*, 2009, **54**, 3059.
5 E. D. Wachsman and K. T. Lee, *Science*, 2011, **334**, 935.
6 Y. Z. Xing, C. J. Li, C. X. Li and G. J. Yang, *J. Power Sources*, 2008, **176**, 31.
7 B. Li, J. Zhang, T. Kaspar, V. Shutthanandan, R. C. Ewing and J. Lian, *Phys. Chem. Chem. Phys.*, 2013, **15**, 1296.
8 J. Wang, Z. Lu, K. Chen, X. Huang, N. Ai, J. Hu, Y. Zhang and W. Su, *J. Power Sources*, 2007, **164**, 17.
9 B. C. H. Steele and A. Heinzel, *Nature*, 2001, **414**, 345.
10 M. A. Laguna-Bercero, *J. Power Sources*, 2012, **203**, 4.
11 A. M. Azad, S. Larose and S. A. Akbar, *J. Mater. Sci.*, 1994, **29**, 4135.
12 P. Ravindran, R. Vidya, A. Kjekshus, H. Fjellvag and O. Eriksson, *Phys. Rev. B: Condens. Matter Mater. Phys.*, 2006, **74**, 224412.
13 K. Brinkman, T. Iuima and H. Takamura, *Jpn. J. Appl. Phys.*, 2007, **46**, L93.
14 E. D. Wachsman, P. Jayaweera, N. Jiang, D. M. Lowe and B. G. Pound, *J. Electrochem. Soc.*, 1997, **144**, 233.
15 D. W. Jung, K. L. Duncan and E. D. Wachsman, *Acta Mater.*, 2010, **58**, 355.
16 M. Leszczynska, X. Lin, W. Wrobel, M. Malys, M. Krynski, S. T. Norberg, S. Hull, F. Krok and I. Abrahams, *Chem. Mater.*, 2013, **25**, 326.
17 B. J. Zeches, M. D. Rossell, J. X. Zhang, A. J. Hatt, Q. He, C.-H. Yang, A. Kumar, C. H. Wang, A. Melville, C. Adamo, G. Sheng, Y.-H. Chu, J. F. Ihlefeld, R. Erni, C. Ederer, V. Gopalan, L. Q. Chen, D. G. Schlom, N. A. Spaldin, L. W. Martin and R. Ramesh, *Science*, 2009, **326**, 977.
18 A. S. Poghossian, H. V. Abovian, P. B. Avakian, S. H. Mkrtchian and V. M. Haroutunian, *Sens. Actuators, B*, 1991, **4**, 545.
19 M. Bibes and A. Barthelemy, *Nat. Mater.*, 2008, **7**, 425.
20 F. Gao, X. Chen, K. Yin, S. Dong, Z. Ren, F. Yuan, T. Yu, Z. Zou and J. M. Liu, *Adv. Mater.*, 2007, **19**, 2889.
21 C. Hengky, X. Moya, N. D. Mathur and S. Dunn, *RSC Adv.*, 2012, **2**, 11843.
22 S. Mohan and B. Subramanian, *RSC Adv.*, 2013, **3**, 23737.
23 Y. Ding, T. H. Wang, W. C. Yang, T. C. Lin, C. S. Tu, Y. D. Yao and K. T. Wu, *IEEE Trans. Magn.*, 2011, **47**, 513.
24 M. M. Kumar, V. R. Palkar, K. Srinivas and S. V. Suryanarayana, *Appl. Phys. Lett.*, 2000, **76**, 2764.
25 Y. P. Wang, L. Zhou, M. F. Zhang, X. Y. Chen and J. M. Liu, *Appl. Phys. Lett.*, 2004, **84**, 1731.
26 S. T. Zhang, M. H. Lu, D. Wu, Y. F. Chen and N. B. Ming, *Appl. Phys. Lett.*, 2005, **87**, 262907.
27 M. S. Bernardo, T. Jardiel, M. Peiteado, A. C. Caballero and M. Villegas, *J. Am. Ceram. Soc.*, 2011, **31**, 3047.
28 J. Wang, J. B. Neaton, H. Zheng, V. Nagarajan, S. B. Ogale, B. Liu, D. Viehland, V. Vaithyanathan, D. G. Schlom, U. V. Waghmare, N. A. Spaldin, K. M. Rabe, M. Wuttig and R. Ramesh, *Science*, 2003, **299**, 1719.
29 Y. Wang, Q. H. Jiang, H. C. He and C. W. Nan, *Appl. Phys. Lett.*, 2006, **88**, 142503.
30 Z. Dai and Y. Akishige, *J. Phys. D: Appl. Phys.*, 2010, **43**, 445403.
31 Y. Teraoka, H. M. Zhang, K. Okamoto and N. Yamazoe, *Mater. Res. Bull.*, 1988, **23**, 51.
32 K. Eguchi, T. Setoguchi, T. Inoue and H. Arai, *Solid State Ionics*, 1992, **52**, 165.
33 M. J. Verkerk, K. Keizer and A. J. Burggraaf, *J. Appl. Electrochem.*, 1980, **10**, 81.
34 W. F. Su, *Principles of Polymer Design and Synthesis*, Springer, 2013, ch. 5.
35 L. Fang, J. Liu, S. Ju, F. Zheng, W. Dong and M. Shen, *Appl. Phys. Lett.*, 2010, **97**, 242501.
36 A. Y. Kim, S. H. Han, H.-W. Kang, H.-G. Lee, J. S. Kim and C. I. Cheon, *Ceram. Int.*, 2012, **38S**, S397.
37 A. R. West, *Basic Solid State Chemistry*, Wiley, 2002, 2nd edn, ch. 7.
38 T. Yamashita and P. Hayes, *Appl. Surf. Sci.*, 2008, **254**, 2441.
39 M. B. Suresh and R. Johnson, *Int. J. Energy Res.*, 2012, **36**, 1291–1297.